CONEM
CONGRESSO NACIONAL DE ENGENHARIA MECÂNICA
NATAL - RIO GRANDE DO NORTE - BRASIL

ABCM
XII CONGRESSO NACIONAL DE ENGENHARIA MECÂNICA
DE 29/07 A 02/08 DE 2024, NATAL-RN, BRASIL

CONEM2024-0218
ANALYSIS OF A MULTIDIRECTIONAL HYBRID ENERGY HARVESTER

Luã Guedes Costa, savi@mecanica.coppe.ufrj.br[1]
Marcelo Amorim Savi, guedes@mecanica.coppe.ufrj.br[1]

[1]Universidade Federal do Rio de Janeiro, COPPE - Mechanical Engineering, Center for Nonlinear Mechanics - Mecanon, Rio de Janeiro, Brazil

Abstract: *Energy harvesting systems play an essential role in contemporary society, and ongoing research in the literature focuses on the development of more efficient designs that allow broader applications. In this regard, one promising approach is the use of hybrid systems that combine multiple transduction mechanisms, such as smart materials, electromagnetic coupling, and triboelectric effect. Another strategy consists of the addition of nonlinear characteristics, which often increase their performance. The source of multidirectionality is another important aspect that still remains a challenging topic. Therefore, the concept and performance of a nonlinear energy harvester that deals with hybrid transduction and multidirectionality is a challenging topic that needs to be investigated. This investigation addresses these challenges by incorporating a pendulum structure in a conventional cantilever-based piezoelectric energy harvester to enable multidirectional capabilities. A generic prototype model is presented to study the main characteristics of this type of system. The performance of the device is addressed and compared to its classical linear cantilever-based counterpart. Results show a significant performance improvement in all scenarios by utilizing the hybrid system.*

Keywords: *Muldidirectional, Hybrid, Energy Harvesting, Pendulum, Electromechanical Systems*

1. INTRODUCTION

Mechanical energy harvesting technology has a wide range of applications across diverse fields within self-powered wireless sensors, IoT (internet of things), and MEMs (micro-electro-mechanical systems). Some examples of the potential applications of mechanical energy harvesting include capturing energy from civil infrastructure motion, implantable biomedical devices, wearables, sea wave energy harvesting, automobiles, and many others (Safaei *et al.*, 2019).

In order to harness the available ambient mechanical energy and effectively convert it into electrical energy, the transduction mechanisms are essential. Electromagnetic converters, triboelectric structures, and piezoelectric materials can be enumerated as some classical strategies to achieve this goal. Electromagnetic harvesters rely on the principle of electromagnetic induction, being commonly used in robust applications, ranging from micro to large scale applications (Cepnik *et al.*, 2013). In contrast, triboelectric structures use friction between two different materials to create an electric potential between two surfaces, making them more compact and suitable for nano to microscale applications (Haroun *et al.*, 2022). On the other hand, piezoelectric materials are smart materials that convert mechanical into electrical energy through the reversible process of the piezoelectric effect, which produces a proportional charge as a result of the application of a mechanical field. Piezoelectric transducers can be applied to harvest energy from micro to large-scale applications (Clementi *et al.*, 2022).

The hybrid transduction combining different types of transducers is a trend to enhance system performance. By combining different types of transducers, the hybridization approach can exploit the unique advantages of each transducer, resulting in greater energy harvesting capacity. Depending on the transducer combinations, various applications can be realized (Chung *et al.*, 2021), and by utilizing the unique advantages of each transducer, hybrid systems can indeed facilitate more efficient energy harvesting solutions.

The harvesters documented in the literature are resonators such as structural elements such as beams and plates. On this basis, their effectiveness in converting energy is limited to situations close to the resonant condition when operating in a linear regime. This limitation has motivated the use of nonlinear modulations, which can increase their operation bandwidth and enable better performance when subjected to environmental uncertainties. Multistable systems that are induced either by magnets or by post-buckled structures can be cited as one of the most common nonlinearity modulations found in the literature (Costa *et al.*, 2021). Compared to the linear systems, this class of harvester presents a better performance by increasing the maximum output power and operation bandwidth (Costa and Savi, 2024; Costa *et al.*,

2024). Nonsmooth impact-driven modulations are also employed to enhance the operation bandwidth, but at the cost of the reduction of the maximum output power (Ai *et al.*, 2019). Besides, the mechanical wear caused by successive impacts can be a drawback of this kind of harvester. Adeodato *et al.* (2021) showed that the synergistic use of smart materials can be a viable solution to control and tune the natural frequency of the harvester, increasing the operation bandwidth in different scenarios. The designs of different structures are also of concern in trying to enhance energy harvesting capacity. In this regard, multimodal structures are proposed with multiple degrees of freedom in order to establish a broadband performance (Caetano and Savi, 2021).

Energy harvesting from multiple directions is another important aspect to be incorporated into the designs since energy sources have unavoidable uncertainties. It has been shown that the usage of pendulum structures to achieve multidirectionality is an interesting and effective solution (Wu *et al.*, 2018). Unlike classical cantilever-based piezoelectric energy harvesters, which primarily operate in a single direction, pendulum-based systems can harness energy from various directions. Pendulum structures have been used in mechanical energy harvesting systems. Specifically, they can be used in some ways to incorporate multidirectional capabilities to the classical cantilever-based piezoelectric energy harvester (Xu and Tang, 2015). Caetano and Savi (2022) proposed a star-shaped harvester, comparing its performance with the counterpart version, without pendula. The proposed harvester presents a multimodal and multidirectional energy harvesting capacity.

This work deals with an investigation of multidirectional mechanical energy harvesting, proposing an archetype reduced order model of a hybrid multidirectional pendulum-based energy harvester (MHEH). Specifically, the MHEH is a modified version of the classical cantilever-based piezoelectric energy harvester. Pendulum-based system presents multidirectional coupling, allowing the conversion of the mechanical energy source directions that otherwise would be lost. A piezoelectric transducer is attached to a cantilever structure to convert energy from flexural oscillations, while an electromagnetic converter is attached to the pendulum to harness the rotational energy. Numerical simulations are performed showing that the usage of pendulum structures together with conventional cantilever-based energy harvesters is advantageous if associated with an additional strategy to harness the rotational energy from the pendulum.

2. DESIGN AND THEORETICAL MODEL

Consider the conceptual representation of three cantilever-based energy harvesters presented in Fig. 1. The first shown in Fig. 1(a), represents the classical cantilever-based piezoelectric energy harvester (CPEH), composed by a piezoelectric transducer attached to a structural beam element, a support where the beam is embedded, and a tip mass at its free end. The second design, displayed in Fig. 1(b), shows the multidirectional piezoelectric harvester (MPEH), which incorporates the pendulum in the classical design. This layout leverages the planar motion of the pendulum to transmit the input energy from one Cartesian direction to another. Finally, Fig. 1(c) displays the proposed multidirectional hybrid energy harvester (MHEH), which incorporates an additional electromagnetic transducer at the support of the pendulum in order to harness its rotational energy.

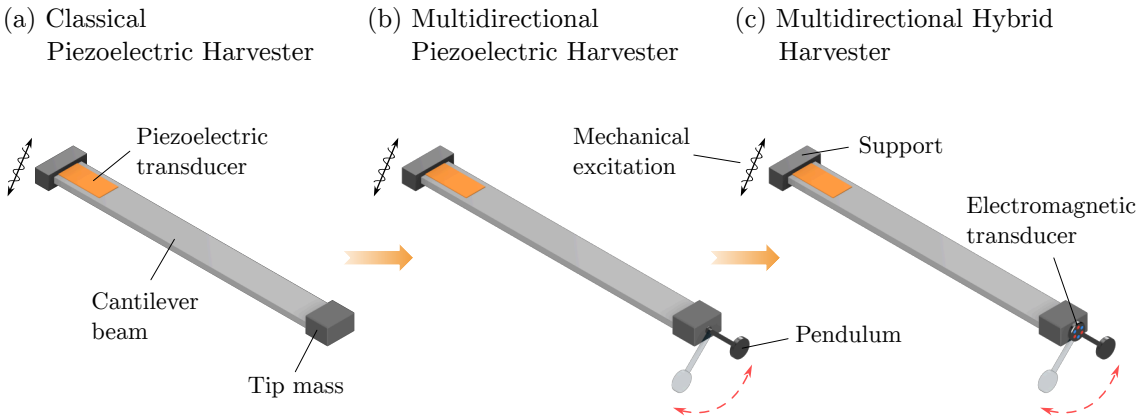

Figure 1: Conceptual representation of the three types of energy harvesters. (a) The classical piezoelectric energy harvester (CPEH), is composed of a piezoelectric transducer and a cantilever beam structure with a tip mass. (b) the multidirectional piezoelectric energy harvester (MPEH), composed by the CPEH plus the addition of a pendulum structure. (c) The proposed multidirectional hybrid energy harvester (MHEH) composed of the MPEH plus the addition of an electromagnetic transducer at the pendulum's support.

2.1 Physical Modeling

In view of the designs presented in Fig. 1, they can be represented by the general archetype model depicted in Fig. 2. The model considers the beam main structure of effective mass m_s, and a pendulum-type element of effective mass m_p attached to it. The equivalent stiffness and damping coefficients are represented by k_i $(i = x, z, pz)$ and c_j $(j = x, z, em, p)$, in which subscripts are related to the direction or an element within the system. Subscript x and z refer to the plane directions, while subscript p refers to the pendulum; subscripts pz and em refer to the piezoelectric

and electromagnetic transducers, respectively. Two transducers are attached to the system: a piezoelectric element with an electromechanical coupling term, θ_{pz} and an equivalent stiffness, k_{pz}, in the z direction of the structure; and an electromagnetic energy converter attached to the support of the pendulum with an electromagnetic coupling term, θ_{em}, and a magnetic damping coefficient c_{em}. The transducers are represented by an equivalent circuit. The piezoelectric element can be represented by a circuit depicted in Fig. 2(b), with an internal capacitance, C_{pz}, connected in parallel to an internal resistance, R_{ipz}, and an induced current related to the electromechanical coupling, $I_{pz}(t) = \theta_{pz}\dot{z}_s(t)$. An external load resistance, R_{lpz}, is also attached to the piezoelectric element. Additionally, the electromagnetic transducer is represented by the circuit depicted in Fig. 2(c), with a voltage source, $v_{em}(t) = \theta_{em}\dot{\phi}(t)$, connected in series with an equivalent internal inductance, L_m, an internal resistance R_{iem}, and an external load resistance, R_{lem}. The equivalent resistance of the piezoelectric circuit is represented by $R_{pz} = R_{ipz}R_{lpz}/\left(R_{lpz} + R_{ipz}\right)$, while the equivalent resistance of the electromagnetic circuit is represented by $R_{em} = R_{iem} + R_{lem}$.

The effects of gravity, g, are considered, and the system is subjected to a multidirectional excitation represented by the vector $\mathbf{r_b}(t) = r_b(t)\left[\sin(\mu)\hat{\mathbf{e}}_x + \cos(\mu)\hat{\mathbf{e}}_z\right]$, where the bold notation refers to vectors and italic notation refers to scalars; μ is the angle between the external excitation vector $\mathbf{r_b}(t)$ and the z direction, and $r_b(t)$ is the excitation function; the vectors $\hat{\mathbf{e}}_x$ and $\hat{\mathbf{e}}_z$ are the base vectors of each Cartesian direction, x and z, respectively.

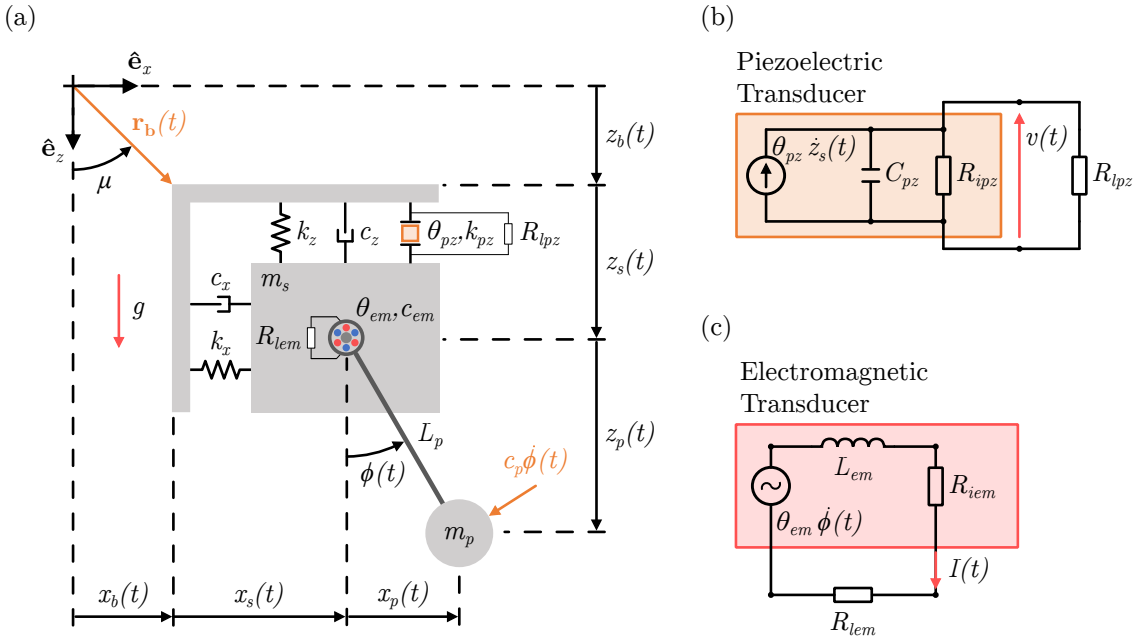

Figure 2: (a) Archetype representing the Hybrid Multidirectional Energy Harvester. (b) The equivalent circuit of the piezoelectric transducer attached to a resistance. (c) The equivalent circuit of the electromagnetic transducer attached to a resistance.

On this basis, the Lagrangian can be defined as $\mathcal{L} = T - U + W$, where T is the kinetic energy, U is the potential energy, and W is the piezoelectric energy. The electromechanical system is associated with five generalized coordinates (three mechanical and two electrical), $\mathbf{Q} = [x(t), z(t), \phi(t), \psi(t), q(t)]$, where $x(t)$ and $z(t)$ are the relative displacement to the base in the horizontal and vertical directions, respectively; $\phi(t)$ is the angular position of the pendulum, $\psi(t)$ is the magnetic flux linkage of the piezoelectric circuit, and $q(t)$ is the electric charge of the electromagnetic circuit. Therefore, by applying the method of Euler-Lagrange where D is the dissipation function, the following equation is achieved,

$$\frac{d}{dt}\left(\frac{\partial \mathcal{L}}{\partial \dot{Q}_i}\right) - \frac{\partial \mathcal{L}}{\partial Q_i} + \frac{\partial D}{\partial \dot{Q}_i} = 0. \tag{1}$$

Suppressing the (t) in the notation of the generalized coordinates, the electromechanical equations of motion can be written as a system of equations dependent of x, z, ϕ, v and I:

$$(m_s + m_p)\,\ddot{x} + c_x\dot{x} + k_x x + m_p L_p\left[\ddot{\phi}\cos(\phi) - \dot{\phi}^2\sin(\phi)\right] = -(m_s + m_p)\,\ddot{x}_b; \tag{2}$$

$$(m_s + m_p)\,\ddot{z} + c_z\dot{z} + (k_z + k_{pzt})\,z - \theta_{pz}v - m_p L_p\left[\ddot{\phi}\sin(\phi) + \dot{\phi}^2\cos(\phi)\right] = -(m_s + m_p)\,\ddot{z}_b; \tag{3}$$

$$m_p L_p^2\ddot{\phi} + (c_{em} + c_p L_p)\dot{\phi} + m_p L_p\left[\ddot{x}\cos(\phi) + (g - \ddot{z})\sin(\phi)\right] - \theta_{em}I = m_p L_p\left[\ddot{z}_b\sin(\phi) - \ddot{x}_b\cos(\phi)\right]; \tag{4}$$

$$C_{pz}\dot{v} + \frac{v}{R_{pz}} + \theta_{pz}\dot{z} = 0; \tag{5}$$

$$L_{em}\dot{I} + R_{em}I + \theta_{em}\dot{\phi} = 0. \tag{6}$$

Assuming a harmonic external stimulus results in the following expressions:

$$\mathbf{r_b} = x_b\hat{\mathbf{e}}_x + z_b\hat{\mathbf{e}}_z = A\sin(\omega t)\left[\sin(\mu)\hat{\mathbf{e}}_x + \cos(\mu)\hat{\mathbf{e}}_z\right], \tag{7}$$

$$\ddot{\mathbf{r}}_\mathbf{b} = \ddot{x}_b\hat{\mathbf{e}}_x + \ddot{z}_b\hat{\mathbf{e}}_z = -A\omega^2\sin(\omega t)\left[\sin(\mu)\hat{\mathbf{e}}_x + \cos(\mu)\hat{\mathbf{e}}_z\right] \tag{8}$$

In order to generalize the analysis of the system, a normalization approach is performed by considering a reference length, L, a reference voltage V, and a reference current $\mathcal{I}$, resulting in the dimensionless electromechanical equations given by:

$$(1+\rho)\,\ddot{\bar{x}} + 2\zeta_x\dot{\bar{x}} + \Omega_s^2\bar{x} + \rho\ell\left[\ddot{\bar{\phi}}\cos(\bar{\phi}) - \dot{\bar{\phi}}^2\sin(\bar{\phi})\right] = -(1+\rho)\ddot{\bar{x}}_b; \tag{9}$$

$$(1+\rho)\,\ddot{\bar{z}} + 2\zeta_z\dot{\bar{z}} + \bar{z} - \chi_{pz}\bar{v} - \rho\ell\left[\ddot{\bar{\phi}}\sin(\bar{\phi}) + \dot{\bar{\phi}}^2\cos(\bar{\phi})\right] = -(1+\rho)\ddot{\bar{z}}_b; \tag{10}$$

$$\ddot{\bar{\phi}} + 2\zeta_\phi\dot{\bar{\phi}} + \Omega_\phi^2\sin(\bar{\phi}) - \chi_{em}\bar{I} + \frac{1}{\ell}\left[\ddot{\bar{x}}\cos(\bar{\phi}) - \ddot{\bar{z}}\sin(\bar{\phi})\right] = \frac{1}{\ell}\left[\ddot{\bar{z}}_b\sin(\bar{\phi}) - \ddot{\bar{x}}_b\cos(\bar{\phi})\right]; \tag{11}$$

$$\dot{\bar{v}} + \frac{\bar{v}}{\varphi_{pz}} + \kappa_{pz}\dot{\bar{z}} = 0; \tag{12}$$

$$\dot{\bar{I}} + \varphi_{em}\bar{I} + \kappa_{em}\dot{\bar{\phi}} = 0. \tag{13}$$

These equations are related to the dimensionless parameters presented in Table 1.

Table 1: System parameters and values used in the analyses

Parameter Description	Symbol	Definition	Value
Natural frequency of the main structure in x	ω_x	$\sqrt{k_x/m_s}$	-
Natural frequency of the main structure in z	ω_z	$\sqrt{k_z/m_s}$	-
Linearized natural frequency of the pendulum	ω_ϕ	$\sqrt{g/L_p}$	-
Normalized time	τ	$\omega_z t$	-
Normalized x displacement of the main structure	$\bar{x}(\tau)$	$x(t)/L$	-
Normalized z displacement of the main structure	$\bar{z}(\tau)$	$z(t)/L$	-
Normalized angle of the pendulum structure	$\bar{\phi}(\tau)$	$\phi(t)$	-
Normalized voltage of the piezoelectric circuit	$\bar{v}(\tau)$	$v(t)/V$	-
Normalized current of the electromagnetic circuit	$\bar{I}(\tau)$	$I(t)/\mathcal{I}$	-
Normalized base excitation frequency	Ω	ω/ω_z	$0.01 \rightarrow 2$
Normalized base excitation amplitude	γ	A/L	$0.1, 0.25, 0.5$
Normalized angle of the base excitation vector $\mathbf{r_b}(t)$	$\bar{\mu}$	μ	$0^\circ, 45^\circ, 90^\circ$
Normalized base excitation displacement in the x direction	$\bar{x}_b(\tau)$	$\gamma\sin(\Omega\tau)\sin(\bar{\mu})$	-
Normalized base excitation displacement in the z direction	$\bar{z}_b(\tau)$	$\gamma\sin(\Omega\tau)\cos(\bar{\mu})$	-
Ratio of masses	ρ	m_p/m_s	0.5
Normalized damping coefficient of the main structure in x	ζ_x	$c_x/(2\omega_z m_s)$	0.025
Normalized damping coefficient of the main structure in z	ζ_z	$c_z/(2\omega_z m_s)$	0.025
Normalized total damping coefficient of the pendulum structure	ζ_ϕ	$\frac{[(c_{em}/L_p)+c_p]}{2\omega_z L_p m_s}$	0.0025
Ratio of natural frequencies of the main structure	Ω_s	ω_x/ω_z	$0.5, 1, 1.5$
Ratio of natural frequencies of the pendulum and the z direction	Ω_ϕ	ω_ϕ/ω_z	0.05
Normalized pendulum length	ℓ	L_p/L	1
Normalized piezoelectric coupling in the mechanical ODE	χ_{pz}	$\theta_{pz}V/(k_z L)$	0.05
Normalized electromagnetic coupling in the mechanical ODE	χ_{em}	$\theta_{em}\mathcal{I}/(\rho k_z L_p^2)$	$\eta\chi_{pz}$
Normalized piezoelectric coupling in the piezo circuit ODE	κ_{pz}	$\theta_{pz}L/(C_{pz}V)$	0.5
Normalized EM coupling in the electromagnetic circuit ODE	κ_{em}	$\theta_{em}/(L_{em}\mathcal{I})$	$\eta\kappa_{pz}$
Normalized equivalent resistance of the piezoelectric circuit	φ_{pz}	$C_{pz}R_{pz}\omega_z$	$0.2 \rightarrow 100$
Normalized equivalent resistance of the electromagnetic circuit	φ_{em}	$R_{em}/(L_{em}\omega_z)$	$0.01 \rightarrow 5$
Ratio between electromechanical couplings	η	$\chi_{em}/\chi_{pz} = \kappa_{em}/\kappa_{pz}$	$0.2 \rightarrow 1.0$
Normalized electrical output power of the piezoelectric circuit	$\bar{P}_{pz}(\tau)$	$P_{pz}(t)/(C_{pz}\omega_z V^2)$	-
Normalized electrical output power of the electromagnetic circuit	$\bar{P}_{em}(\tau)$	$P_{em}(t)/(L_{em}\omega_z\mathcal{I}^2)$	-

2.2 Performance Metrics

The performance of the energy harvesting system is evaluated with the definition of the electrical power associated with both piezoelectric and electromagnetic circuits. The total instantaneous electrical power consists of the sum of the instantaneous electrical power, P, in each circuit. Thus, the average electrical power, defined over the interval $t_0 \leq t \leq t_f$, is represented by Equation 14, where v^{RMS} and I^{RMS} are the root-mean-square (RMS) of the output voltage of the piezoelectric circuit and of the output current of the electromagnetic circuit, respectively.

$$P_{\mathrm{avg}} = \frac{1}{t_f - t_0}\int_{t_0}^{t_f} P\,dt = \frac{1}{R_{pz}}\left(v^{\mathrm{RMS}}\right)^2 + R_{em}\left(I^{\mathrm{RMS}}\right)^2, \tag{14}$$

Furthermore, based on these concepts and according to Table 1, the normalized average electrical output power can be determined as described in Equation 15.

$$\bar{P}_{\mathrm{avg}} = \bar{P}_{pz} + \bar{P}_{\mathrm{em}} = \frac{1}{\varphi_{pz}}\left(\bar{v}^{\mathrm{RMS}}\right)^2 + \varphi_{em}\left(\bar{I}^{\mathrm{RMS}}\right)^2. \tag{15}$$

Numerical simulations carried out employing the fourth order Runge-Kutta scheme, considering a time step $\Delta\tau \propto 2\pi/\Omega$ defined after a convergence analysis. Dynamical observations are treated together with performance.

3. Characterization of the MHEH Performance

The performance of the HMEH is evaluated and the electromechanical couplings of the electromagnetic transducer, χ_{em} and κ_{em}, are important to be addressed. The value of these couplings is influenced by many construction characteristics of the transducer, especially the disposal of coils and internal magnet properties. In order to perform a general qualitative analysis of the MHEH, a variable is defined containing information of the electromagnetic transducer, based on the piezoelectric transducer. On this basis, consider the ratio between electromechanical couplings as $\eta = \chi_{em}/\chi_{pz} = \kappa_{em}/\kappa_{pz}$, where it is noticeable that if $\eta = 1$, both transducers have the same coupling, while if $\eta < 1$, electromagnetic couplings have a lower value than the corresponding piezoelectric coupling. Alternatively, if $\eta > 1$, the electromagnetic couplings have a larger value than the corresponding piezoelectric couplings.

This section develops a characterization of the system's performance by evaluating the influence of different parameters. The first subsection evaluates the influence of the electrical resistance parameters on the output power. On the other hand, the second subsection performs the comparison between the proposed MHEH and the CPEH, utilizing a fixed value of η. The analyses are carried out by considering three different configurations with different ratios of natural frequencies. The first configuration is characterized by $\Omega_s = 0.5$, while the second is characterized by $\Omega_s = 1.0$, and the third by $\Omega_s = 1.5$. An illustrative representation of the Ω_s parameter is presented in Fig. 3. The angle of excitation is maintained constant at $\bar{\mu} = 45°$. The values of the remaining parameters are summarized in Table 1.

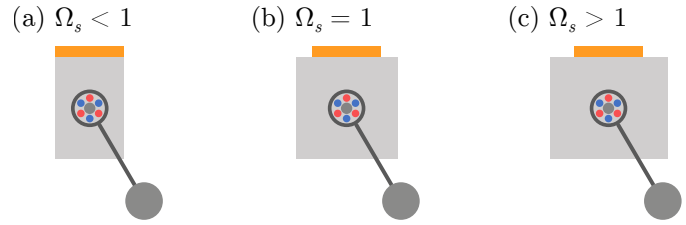

Figure 3: Illustrative representation of the ratio of natural frequencies, Ω_s. (a) $\Omega_s < 1$, where the $\bar{x}$ direction is softer than the $\bar{z}$ direction, that is, the beam's width is shorter than its height. (b) $\Omega_s = 1$, where both $\bar{x}$ and $\bar{z}$ directions have the same stiffness, that is, both beam's width and height have the same length. (c) $\Omega_s > 1$, where the $\bar{x}$ direction is stiffer than the $\bar{z}$ direction, that is, the beam's width is larger than its height.

3.1 Influence of the Electrical Resistances, φ_{pz} and φ_{em}

In this subsection, the influence of the electrical resistance parameters is of concern, establishing the effect on the average output power of the system. By considering a constant value of $\eta = 1$ and $\gamma = 0.1$, Average Output Power Diagrams (OPDs) are constructed to analyze the influence of the normalized electrical resistance parameters, φ_{pz}, and φ_{em}, and the excitation frequency, Ω, in the output power of the system, as shown in Fig. 4.

Three configurations with different values of Ω_s are chosen. Each column of Fig. 4 is related to one different configuration: Fig. 4(a) for $\Omega_s = 0.5$, that is, the $\bar{z}$ direction is stiffer than the $\bar{x}$ direction; Fig. 4(b) for $\Omega_s = 1.0$, where both stiffness of each direction are equal; and Fig. 4(c) for $\Omega = 1.5$, showing a configuration with a stiffer $\bar{x}$ direction than the $\bar{z}$ direction. The first row of each configuration shows the OPD for the values of the normalized conductance of the piezoelectric circuit, $1/\varphi_{pz}$. For all configurations, the optimal value of the normalized conductance is shown to be around $1/\varphi_{pz} = 1$. Additionally, the second row of each configuration shows the OPD for the values of the normalized resistance of the electromagnetic circuit, φ_{em}. As in the previous case, the three configurations show similar regions of optimal resistance around $\varphi_{em} = 0.25$.

In this case, it should be pointed out that the increase of Ω_s produces an increase in the maximum output power of both piezoelectric and electromagnetic transducers. Additionally, the presence of two peaks of output power in the first and third cases, as shown by white arrows, occur due to the shift of the resonance regions provoked by the change in Ω_s.

3.2 MHEH vs CPEH

In this subsection, the comparison of the performance between the proposed multidirectional hybrid energy harvester (MHEH) and the classic piezoelectric energy harvester (CPEH) is of concern. As in the previous subsection, three values of Ω_s are evaluated: $\Omega_s = 0.5$, $\Omega_s 1.0$, and $\Omega_s = 1.5$. Results are summarized in $\bar{P}_{\text{avg}} \times \Omega$ diagrams displayed in Fig. 5, which are divided into three sections based on different values of normalized excitation amplitude of $\gamma = 0.1$, $\gamma = 0.25$, and $\gamma = 0.5$. Dashed lines represent the $\bar{P}_{\text{avg}}$ for the CPEH, serving as a reference for comparison. Additionally, these diagrams include red curves that represent the average output power associated with the piezoelectric element, $\bar{P}_{pz}$, orange curves that represent the average output power of the electromagnetic transducer, $\bar{P}_{em}$, and purple curves that represent the total average output power of the MHEH, $\bar{P}_{\text{avg}}$. Note that all values of power are scaled by $\times 10^3$ for better representation. Results illustrate the case where the value of η is increased to 0.8. In this case, nearly all combinations of Ω_s and γ demonstrate the benefits of employing the MHEH. This is due to the fact that, in the whole scenario, the output powers are comparable to or exceed those presented by the CPEH. Given this set of parameters, both piezoelectric and electromagnetic transducers contribute effectively to the energy conversion. For higher values of η, the electromagnetic transducer should convert much more than the piezoelectric element. On the other hand, for lower values of η, the

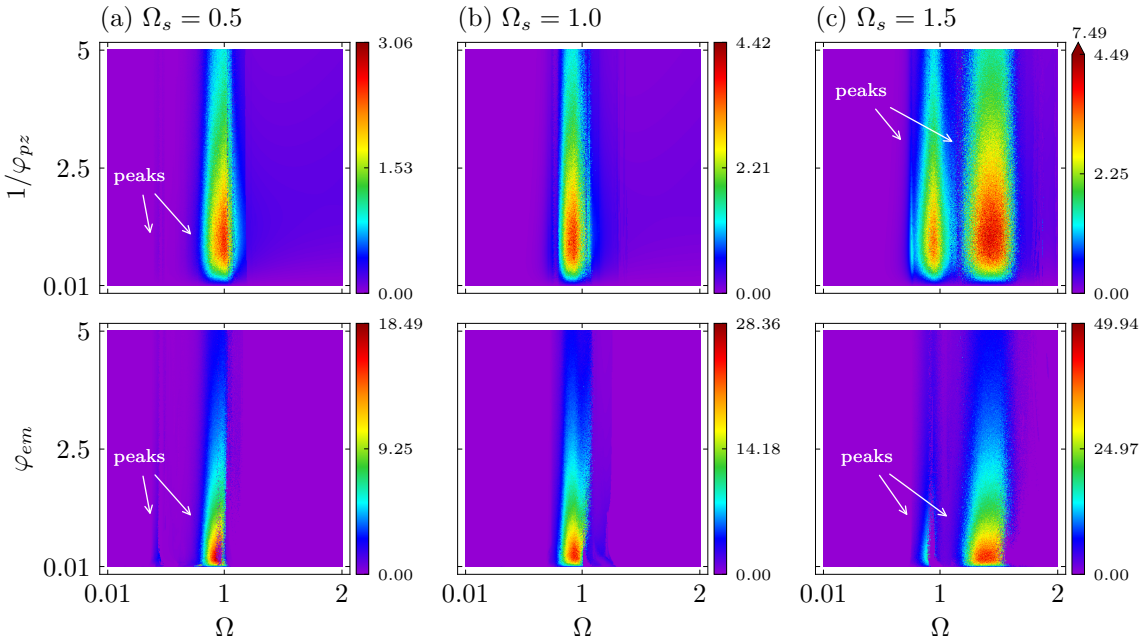

Figure 4: OPDs for the normalized electrical resistance analysis, using a normalized excitation amplitude of $\gamma = 0.1$ and excitation angle of $\bar{\mu} = 45°$. Three groups with different ratios of natural frequencies of the main structure are defined: (a) with $\Omega_s = 0.5$, (b) $\Omega_s = 1.0$, and (c) $\Omega_s = 1.5$. Each group has two rows: The first row shows the output power for different values of conductance of the piezoelectric circuit ($1/\varphi_{pz}$), while the second row shows the output power for different values of the resistance of the electromagnetic circuit (φ_{em}). Rainbow colors in the colorbar indicate the level of average output power, $\bar{P}_{\text{avg}}$, achieved in each case. Colorbars that have an arrow at the top indicate that the range of colorbar values was limited for better display and the top value above the arrow is the maximum output power achieved. All values of $\bar{P}_{\text{avg}}$ are scaled by $\times 10^3$.

piezoelectric transducer should convert more than the piezoelectric element. Finally, it is noticeable that the values of output power presented in Fig. 5 and Fig. 4 reveal that by increasing Ω_s, promote the increase of the bandwidths.

4. CONCLUSIONS

This work presents a novel hybrid multidirectional energy harvester (HMEH) that is able to enhance the performance of cantilever-based harvesters when subjected to multidirectional excitations. The proposed system employs a pendulum structure to achieve multidirectionality and multiple transduction mechanisms to enhance energy conversion. Specifically, a piezoelectric transducer is attached to the cantilever structure, and an electromagnetic transducer is incorporated into the rotational support of the pendulum.

A theoretical model is established to describe the qualitative characteristics of the MHEH and numerical simulations are carried out in order to characterize its performance by analyzing key parameters. Initially, the optimal resistance parameters are identified in order to find the maximum output power regions of both transducers. Using the optimal resistance values, it is demonstrated that the ratio of electromechanical couplings ($\eta = \chi_{em}/\chi_{pz} = \kappa_{em}/\kappa_{pz}$) should be approximately 0.8 for both piezoelectric and electromagnetic transducers to effectively contribute to energy conversion. If this ratio is too low, the piezoelectric element dominates the energy conversion, whereas if η is too high, the electromagnetic transducer converts more energy than the piezoelectric element. Furthermore, it is observed that the electromagnetic transducer predominantly handles the energy conversion at low excitation amplitudes. Alternatively, the piezoelectric transducer takes precedence in energy conversion as the excitation amplitudes increase.

Finally, the natural frequencies of the structure (the natural frequencies in each direction of the Cartesian plane) are evaluated. Results show that a stiffer horizontal direction (perpendicular to the direction of gravity) enhances the bandwidth of the system. Overall, this study shows that the HMEH demonstrates an impressive increase in performance in both maximum output power and bandwidth when compared to its classical linear counterpart.

5. ACKNOWLEDGEMENTS

The authors would like to acknowledge the support of the Brazilian Research Agencies CNPq, CAPES, and FAPERJ and through INCT -Smart Structures in Engineering, CNPq, CAPES and FAPEMIG. The support from the AFOSR and the computational resources of NACAD are also acknowledged.

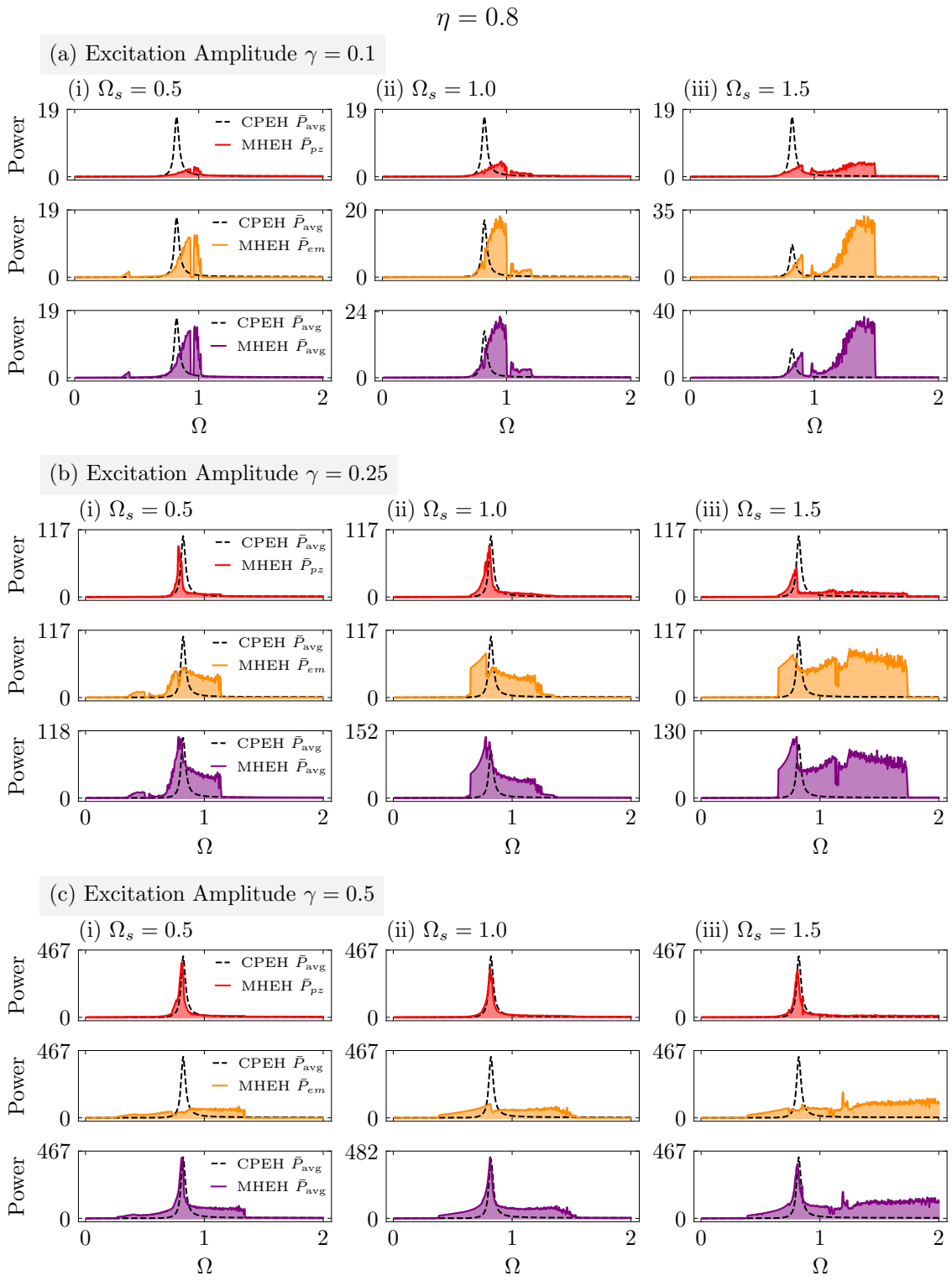

Figure 5: $\bar{P}_{\text{avg}} \times \Omega$ diagrams for $\eta = 0.5$. Three excitation amplitude values are chosen: (a) $\gamma = 0.1$, (b) $\gamma = 0.25$, and (c) $\gamma = 0.5$. For each value of γ, three configurations are selected with (i) $\Omega_s = 0.5$, (ii) $\Omega_s = 1$ and (iii) $\Omega_s = 1.5$. In each plot, dashed lines represent the $\bar{P}_{\text{avg}}$ for the CPEH, serving as a reference for comparison. Additionally, red curves represent $\bar{P}_{pz}$, orange curves represent $\bar{P}_{em}$, and purple curves represent $\bar{P}_{\text{avg}}$, all for the MHEH. All values of power are scaled by $\times 10^3$.

6. REFERENCES

Adeodato, A., Duarte, B.T., Monteiro, L.L.S., Pacheco, P.M.C. and Savi, M.A., 2021. "Synergistic use of piezoelectric and shape memory alloy elements for vibration-based energy harvesting". *International Journal of Mechanical Sciences*, Vol. 194, p. 106206. ISSN 0020-7403. doi:10.1016/j.ijmecsci.2020.106206. URL `https://www.sciencedirect.com/science/article/pii/S0020740320343113`.

Ai, R., Monteiro, L.L.S., Monteiro, P.C.C., Pacheco, P.M.C.L. and Savi, M.A., 2019. "Piezoelectric vibration-based

energy harvesting enhancement exploiting nonsmoothness". *Actuators*, Vol. 8, No. 1. ISSN 2076-0825. doi: 10.3390/act8010025. URL https://www.mdpi.com/2076-0825/8/1/25.

Caetano, V.J. and Savi, M.A., 2021. "Multimodal pizza-shaped piezoelectric vibration-based energy harvesters". *Journal of Intelligent Material Systems and Structures*, Vol. 32, No. 20, pp. 2505–2528. doi:10.1177/1045389X211006910. URL https://doi.org/10.1177/1045389X211006910.

Caetano, V.J. and Savi, M.A., 2022. "Star-shaped piezoelectric mechanical energy harvesters for multidirectional sources". *International Journal of Mechanical Sciences*, Vol. 215, p. 106962. ISSN 0020-7403. doi:https://doi.org/10.1016/j.ijmecsci.2021.106962. URL https://www.sciencedirect.com/science/article/pii/S002074032100672X.

Cepnik, C., Lausecker, R. and Wallrabe, U., 2013. "Review on electrodynamic energy harvesters—a classification approach". *Micromachines*, Vol. 4, No. 2, pp. 168–196. ISSN 2072-666X. doi:10.3390/mi4020168. URL https://www.mdpi.com/2072-666X/4/2/168.

Chung, J., Song, M., Chung, S.H., Choi, W., Lee, S., Lin, Z.H., Hong, J. and Lee, S., 2021. "Triangulated cylinder origami-based piezoelectric/triboelectric hybrid generator to harvest coupled axial and rotational motion". *Research*, Vol. 2021. doi:10.34133/2021/7248579. URL https://spj.science.org/doi/abs/10.34133/2021/7248579.

Clementi, G., Cottone, F., Di Michele, A., Gammaitoni, L., Mattarelli, M., Perna, G., López-Suárez, M., Baglio, S., Trigona, C. and Neri, I., 2022. "Review on innovative piezoelectric materials for mechanical energy harvesting". *Energies*, Vol. 15, No. 17. ISSN 1996-1073. doi:10.3390/en15176227. URL https://www.mdpi.com/1996-1073/15/17/6227.

Costa, L.G., Monteiro, L.L.S. and Savi, M.A., 2024. "Multistability investigation for improved performance in a compact nonlinear energy harvester". *Journal of the Brazilian Society of Mechanical Sciences and Engineering*, Vol. 46, No. 4, p. 212. ISSN 1806-3691. doi:10.1007/s40430-024-04766-5. URL https://doi.org/10.1007/s40430-024-04766-5.

Costa, L.G. and Savi, M.A., 2024. "Nonlinear dynamics of a compact and multistable mechanical energy harvester". *International Journal of Mechanical Sciences*, Vol. 262, p. 108731. ISSN 0020-7403. doi:10.1016/j.ijmecsci.2023.108731. URL https://www.sciencedirect.com/science/article/pii/S0020740323006331.

Costa, L.G., da Silva Monteiro, L.L., Pacheco, P.M.C.L. and Savi, M.A., 2021. "A parametric analysis of the nonlinear dynamics of bistable vibration-based piezoelectric energy harvesters". *Journal of Intelligent Material Systems and Structures*, Vol. 32, No. 7, pp. 699–723. doi:10.1177/1045389X20963188. URL https://doi.org/10.1177/1045389X20963188.

Haroun, A., Tarek, M., Mosleh, M. and Ismail, F., 2022. "Recent progress on triboelectric nanogenerators for vibration energy harvesting and vibration sensing". *Nanomaterials*, Vol. 12, No. 17. ISSN 2079-4991. doi:10.3390/nano12172960. URL https://www.mdpi.com/2079-4991/12/17/2960.

Safaei, M., Sodano, H.A. and Anton, S.R., 2019. "A review of energy harvesting using piezoelectric materials: state-of-the-art a decade later (2008–2018)". *Smart Materials and Structures*, Vol. 28, No. 11, p. 113001. doi:10.1088/1361-665X/ab36e4. URL https://dx.doi.org/10.1088/1361-665X/ab36e4.

Wu, Y., Qiu, J., Zhou, S., Ji, H., Chen, Y. and Li, S., 2018. "A piezoelectric spring pendulum oscillator used for multi-directional and ultra-low frequency vibration energy harvesting". *Applied Energy*, Vol. 231, pp. 600–614. ISSN 0306-2619. doi:10.1016/j.apenergy.2018.09.082. URL https://www.sciencedirect.com/science/article/pii/S030626191831393X.

Xu, J. and Tang, J., 2015. "Multi-directional energy harvesting by piezoelectric cantilever-pendulum with internal resonance". *Applied Physics Letters*, Vol. 107, No. 21. ISSN 0003-6951. doi:10.1063/1.4936607. URL https://doi.org/10.1063/1.4936607. 213902.

7. RESPONSIBILITY NOTICE

The authors are solely responsible for the printed material included in this paper.